MOLECULAR PHYSICS, 1976, VOL. 31, NO. 1, 265–287

Beam maser spectrum of the $1_{11} \rightarrow 1_{01}$ transition of ND_2H and the hyperfine structure of the ammonia molecule†

by R. MICHAEL GARVEY and FRANK C. DE LUCIA
Department of Physics, Duke University, Durham, North Carolina 27706

and JAMES W. CEDERBERG
Department of Physics, St. Olaf College, Northfield, Minnesota 55057

(*Received* 30 *June* 1975)

The structure of the $1_{11} \rightarrow 1_{01}$ transition of ND_2H has been studied by means of millimetre-wave beam maser spectroscopy. Twenty-five components which result from the nitrogen, deuterium, and hydrogen hyperfine interactions have been resolved and theoretically analysed. The theory of three identical particles is discussed and used to fit the beam maser spectra of the $J=K=4$ and $J=K=6$ inversion transitions of ND_3 which have been reported previously. These results are compared with those of the submillimetre-wave beam maser spectrum of the $J=1 \rightarrow 0$ transition of ND_3. By use of molecular and isotopic relations, the results of this work are critically compared with previous centimetre-wave beam maser studies of NH_3 and NH_2D.

1. INTRODUCTION

Of all of the molecules studied by beam maser techniques, none has been investigated as extensively as ammonia. Gordon [1] used the first molecular beam maser to resolve much of the hyperfine structure of the NH_3 species and Kukolich [2–4] later reinvestigated this species under higher resolution. NH_2D has been studied both by Thaddeus *et al.* [5] and by Kukolich [6] in the cm-wavelength region of the spectrum. Basov and Bashkin [7] and Zuev [8] have reported beam maser measurements of the hyperfine structure of the ND_3 inversion spectrum in the 1·6 GHz region. The structure of the $J=1 \rightarrow 0$ rotation–inversion transition of this species at 309 GHz has recently been reported by Garvey and De Lucia [9]. Nevertheless, numerous inconsistencies and uncertainties remain among the interpretations of the results of these experiments.

In this paper are reported the results of a millimetre-wave beam maser study of the hyperfine structure of the $1_{11} \rightarrow 1_{01}$ transition of ND_2H. This study provides important additional information about the role of both the deuterium quadrupole and hydrogen spin–rotation coupling in the hyperfine structure of the ammonia molecule. In addition, the hyperfine structures of ND_3 reported in references [7] and [8] are analysed by the techniques of Cederberg [10]. Previous analyses of these spectra [7, 11] have resulted both in hyperfine constants which are inconsistent with the results of other beam maser studies of ammonia and in poor agreement between the observed and calculated spectra.

† This work was supported by the Army Research Office, Grant Number DAHC0474G0034.

2. Theory—General Considerations

2.1. *Energy levels and transition intensities*

The isotopic species of ammonia exhibit complex hyperfine structure due to the interactions of the electric and magnetic multipole moments of the nuclei with their molecular environment. The theory of these interactions has been considered in several papers and only the results of this theory will be presented here [10–13].

In general, the hyperfine hamiltonian can be represented as

$$\mathscr{H}_{\mathrm{hfs}} = \sum_n \left(\tfrac{1}{6}\mathbf{V}_n \cdot \mathbf{Q}_n + \mathbf{I}_n \cdot \mathbf{C}_n \cdot \mathbf{J}\right) + \sum_n \sum_{m \neq n} \left(\mathbf{I}_n \cdot \mathbf{D}_{nm} \cdot \mathbf{I}_m\right), \tag{1}$$

where contributions from electric quadrupole $\frac{1}{6}\mathbf{V}_n \cdot \mathbf{Q}_n$, magnetic dipole $\mathbf{I}_n \cdot \mathbf{C}_n \cdot \mathbf{J}$, and spin–spin $\mathbf{I}_n \cdot \mathbf{D}_{nm} \cdot \mathbf{I}_m$ interactions are included and where n and m run over all coupling nuclei.

The matrix elements of the electric quadrupole and magnetic dipole interactions may be obtained directly from the relations of reference [12] for several common representations and the general techniques of this reference allow the straightforward calculation of matrix elements in other representations.

Although the energy levels which result from the diagonalization of the hamiltonian matrix are independent of the representation, significant simplifications can result from a judicious selection of this representation. In general, it is advantageous to couple the angular momenta in the order of decreasing interaction energy of the nuclei. In addition, it is useful to couple identical nuclei together prior to their introduction into the rest of the coupling scheme. This latter procedure simplifies the introduction of the special restrictions associated with identical particles. Calculation of transition frequencies from energy levels is straightforward.

In addition to the transition frequencies, the intensity of each hyperfine component must be calculated. First-order transition intensities can be calculated in a straightforward manner from the relations of reference [12]. If the F_i of the coupling scheme are not good quantum numbers, the first-order transition intensity matrix C must be transformed by [13]

$$C' = A_{\mathrm{U}} C A_{\mathrm{L}}^{-1}, \tag{2}$$

where A_{U} and A_{L} are the matrices which diagonalize the hyperfine hamiltonians for the upper and lower rotational states respectively. In beam maser experiments several experimental effects modify the observed intensities. These effects are discussed in § 3.3.

2.2. *Molecular relations*

Under the assumption that isotopic substitution leaves the molecular structure unchanged and if vibrational and centrifugal distortion effects are neglected, the spectroscopic constants of the several isotopic species can be related to more fundamental molecular parameters as well as to each other. For the quadrupole interaction, it is possible to relate q_J, the spectroscopic constant, to V_{gg}, the components of the electric field gradient along the principal axes of the moment of inertia, by

$$q_J = \frac{2J}{2J+3} \sum_g \frac{\langle P_g^2 \rangle}{J(J+1)} V_{gg}, \tag{3}$$

where g refers to the principal axes of the moment of inertia tensor and P_g is the rotational angular momentum component along the g-axis. Similarly,

$$C_J = g_I \sum_g \frac{\langle P_g^2 \rangle}{J(J+1)} \Lambda_{gg} B_g, \tag{4}$$

where C_J is the spin–rotation constant for the J state, g_I is the nuclear g-factor, B_g is the rotational constant for the g-axis and $\mathbf{\Lambda}$ is a tensor which relates to the magnetic field produced at the nuclear site by the molecular rotation. The products $g_I \Lambda_{gg} B_g$ are the quantities generally referred to as the diagonal elements of the spin–rotation tensor C_{gg}. Under the above assumptions both $\mathbf{V}$ and $\mathbf{\Lambda}$ are molecular tensors and are independent of isotopic substitution. For the symmetric top these reduce to

$$q_J = q \frac{J}{2J+3} \left(\frac{3K^2}{J(J+1)} - 1 \right) \tag{5}$$

and

$$C_J = C_N + (C_K - C_N) \frac{K^2}{J(J+1)}, \tag{6}$$

where

$$V_{zz} = q, \quad V_{xx} + V_{yy} + V_{zz} = 0, \quad \frac{C_{xx} + C_{yy}}{2} = C_N$$

and

$$C_{zz} = C_K.$$

3. Hyperfine Structure of the 1_{11}–1_{01} transition of ND_2H

3.1. *Experimental*

In the shorter millimetre and submillimetre region of the microwave spectrum, tunable Fabry–Perot cavities offer significant advantages over the closed cylindrical cavities which are ordinarily used in longer wavelength beam masers. Among these are higher Q, a longer interaction region for the molecular beam and the microwave field, and a significantly larger area through which the molecular beam may be admitted to the cavity. In order to make use of this last factor, a number of molecular beams were generated by effusion through clusters of short sections of needle tubing. These clusters were directed so that the beam from each cluster entered an electrostatic quadrupole state selector. The multiple cluster arrangement produced, with the associated stacked quadrupole state selectors, multiple beams which entered the tunable Fabry–Perot cavity.

All measurements for this work were made with the effusive source described above. This was subsequently modified to a nozzle source of very simple design. Circular holes 0·38 mm in diameter were drilled in 0·25 mm brass sheet. Channels cooled to liquid nitrogen temperature served to collimate these beams. When driven by a pressure of 20–30 torr the nozzle source proved superior to the effusive source, increasing the maser output by a factor of 5–10.

One 57·6 GHz klystron, frequency modulated at 30 MHz, produced a low-level sideband to excite the Fabry–Perot cavity while the fundamental klystron frequency served as the local oscillator for the sensitive super-heterodyne receiver [14]. Since saturation of the rotational transitions occurs at relatively low-field intensities, the power level of this sideband was more than adequate.

An audio-frequency modulation applied to the klystron provided a modulation of the receiver output which could be detected in a phase sensitive amplifier. Details of the construction and operation of a similar maser spectrometer may be found in reference [18].

The narrow linewidths associated with beam spectroscopy placed stringent requirements on frequency accuracy and stability throughout the spectrometer. The klystron must be stabilized and a measurement of its frequency must be made. The reference for both these processes was a General Radio 115-B high stability 5 MHz crystal oscillator continually compared to WWVB by a Hewlett–Packard 117A VLF receiver and phase comparator. This reference was multiplied to form a 180 MHz comb spectrum and mixed with the klystron signal in a 1N26 diode. Various monitors provided frequency measurement and frequency stabilizing signals to be fed back to the klystron.

The sample of ND_2H was prepared by mixing commercial grade anhydrous NH_3 with D_2O in the mole ratio of 1 : 3. The NH_3 readily dissolves in the D_2O, forming a mixture in which hydrogen and deuterium exchange. Fractional distillation and drying remove the water, yielding a mixture of ND_3, ND_2H, NDH_2 and NH_3 in the ratio of 8 : 12 : 6 : 1. The fraction of ND_2H is thus slightly less than half but maximized.

3.2. *Spectral analysis*

ND_2H is a light asymmetric rotor with low J rotational transitions falling in the millimetre and submillimetre wavelength region of the spectrum. The nuclear hyperfine splittings of these low J rotational transitions are both larger than those of higher J rotational transitions, and also less affected by centrifugal distortion. These distortion effects have been shown to be substantial for the light asymmetric rotor HDO [15].

The $1_{11} \rightarrow 1_{01}$ rotation–inversion spectrum at 57 674 MHz is split by the nitrogen hyperfine interaction into five lines which are easily resolvable in an absorption spectrometer. Under higher resolution each of these lines forms a multiplet, composed of several lines which arise due to the hydrogen and deuterium interactions. Lines within the multiplet are typically formed from several closely spaced transitions. The observed hyperfine spectrum is shown in figures 1–6. To prevent confusion in terminology, the above distinction between spectrum, line, multiplet and transition will be adhered to in this work.

The hyperfine hamiltonian which describes this spectrum can be written as

$$\mathscr{H}_{\mathrm{hfs}} = \tfrac{1}{6}\mathbf{V}_{\mathrm{N}} \cdot \mathbf{Q}_{\mathrm{N}} + \mathbf{I}_{\mathrm{N}} \cdot \mathbf{C}_{\mathrm{N}} \cdot \mathbf{J} + \sum_{i=1}^{2} (\tfrac{1}{6}\mathbf{V}_{\mathrm{D}_i} \cdot \mathbf{Q}_{\mathrm{D}_i}) + \sum_{i=1}^{2} (\mathbf{I}_{\mathrm{D}_i} \cdot \mathbf{C}_{\mathrm{D}_i} \cdot \mathbf{J})$$
$$+ \mathbf{I}_{\mathrm{H}} \cdot \mathbf{C}_{\mathrm{H}} \cdot \mathbf{J} + \mathbf{I}_{\mathrm{D}_1} \cdot \mathbf{D}_{\mathrm{D}_1\mathrm{D}_2} \cdot \mathbf{I}_{\mathrm{D}_2} + \sum_{i=1}^{2} (\mathbf{I}_{\mathrm{N}} \cdot \mathbf{D}_{\mathrm{ND}_i} \cdot \mathbf{I}_{\mathrm{D}_i}) + \mathbf{I}_{\mathrm{N}} \cdot \mathbf{D}_{\mathrm{NH}} \cdot \mathbf{I}_{\mathrm{H}}$$
$$+ \sum_{i=1}^{2} (\mathbf{I}_{\mathrm{D}_i} \cdot \mathbf{D}_{\mathrm{D}_i\mathrm{H}} \cdot \mathbf{I}_{\mathrm{H}}). \quad (7)$$

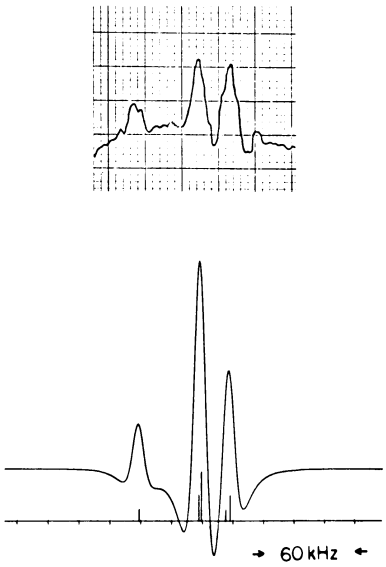

Figure 1. Experimental and theoretical spectrum for the $F_N = 0 \rightarrow 1$ of the $1_{11} \rightarrow 1_{01}$ transition of ND_2H.

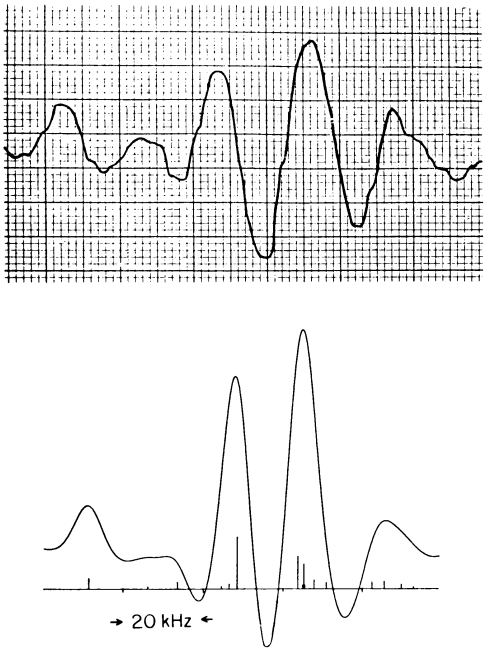

Figure 2. Experimental and theoretical spectrum for the $F_N = 2 \rightarrow 1$ of the $1_{11} \rightarrow 1_{01}$ transition of ND_2H.

The hyperfine constants which correspond to the terms of this hamiltonian are the nitrogen quadrupole $(eq_J Q)_N$, nitrogen spin rotation $(C_J)_N$, deuterium quadrupole $(eq_J Q)_D$, deuterium spin rotation $(C_J)_D$, hydrogen spin rotation $(C_J)_H$, nitrogen–deuterium spin–spin SS_{ND}, deuterium–deuterium spin–spin SS_{DD}, nitrogen–hydrogen spin–spin SS_{NH}, and the deuterium–hydrogen spin–spin SS_{DH}. In general, these constants are different for the 1_{11} and 1_{01} states.

A representation must be selected for the evaluation of the matrix elements of this hamiltonian. The most convenient representation is

$$\mathbf{J}+\mathbf{I}_N = \mathbf{F}_N, \tag{8 a}$$

$$\mathbf{I}_{D_1}+\mathbf{I}_{D_2}=\mathbf{I}_D, \tag{8 b}$$

$$\mathbf{F}_N+\mathbf{I}_D = \mathbf{F}_D, \tag{8 c}$$

$$\mathbf{F}_D+\mathbf{I}_H = \mathbf{F}_H=\mathbf{F}, \tag{8 d}$$

where $\mathbf{J}$ is the rotational angular momentum, $\mathbf{I}_N$, $\mathbf{I}_{D_1}$, $\mathbf{I}_{D_2}$, and $\mathbf{I}_H$ are angular momenta of the nuclei, and where the rest of the angular momenta are defined by the representation. Because the two deuterium nuclei occupy identical sites, I_D can have only the value 1 for the rotation–vibration states considered here. The matrix elements of the electric quadrupole and magnetic dipole interactions of the hamiltonian of equation (7) may be obtained directly from the relations of reference [12] if minor modifications are made which result from the identical deuterium nuclei. The only effect of introducing the identical particles into the coupling scheme via equation (8 *b*) is to require an extra reduction of the

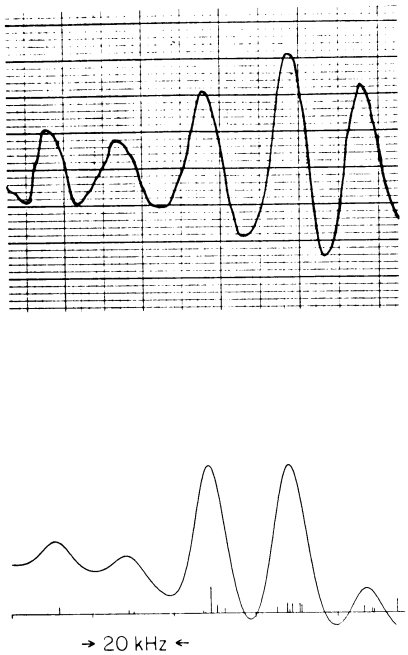

Figure 3. Experimental and theoretical spectrum for the $F_N = 1 \rightarrow 1$ of the $1_{11} \rightarrow 1_{01}$ transition of ND_2H.

reduced matrix elements which involve the individual deuterium spins :

$$\langle I_D \| Q_{D_1} \| I_D \rangle = (-)^{I_{D_1}+I_{D_2}+I_D+2}(2I_D+1)\begin{Bmatrix} I_{D_2} & I_D & I_{D_1} \\ I_D & I_{D_2} & 2 \end{Bmatrix}\langle I_{D_1} \| Q_{D_1} \| I_{D_1} \rangle$$

$$= -\tfrac{1}{2}\langle I_{D_1} \| Q_{D_1} \| I_{D_1} \rangle \quad (\text{for } I_{D_1}=I_{D_2}=I_D=1), \tag{9}$$

$$\langle I_D \| I_{D_1} \| I_D \rangle = (-)^{I_{D_1}+I_{D_2}+I_D+1}(2I_D+1)\begin{Bmatrix} I_{D_2} & I_D & I_{D_1} \\ I_D & I_{D_2} & 1 \end{Bmatrix}\langle I_{D_1} \| I_{D_1} \| I_{D_1} \rangle$$

$$= \tfrac{1}{2}\langle I_{D_1} \| I_{D_1} \| I_{D_1} \rangle \quad (\text{for } I_{D_1}=I_{D_2}=I_D=1). \tag{10}$$

Since there are two coupling nuclei, the only effect on the matrix elements is to introduce a minus one in the matrix elements of the deuterium quadrupole coupling.

The matrix elements of the spin–spin terms of the hamiltonian may be derived by use of these same techniques. The hamiltonian for the spin–spin interaction can be written as

$$\mathscr{H} = \mathbf{I}_1 \cdot \mathbf{D}_{12} \cdot \mathbf{I}_2, \tag{11}$$

where $\mathbf{D}_{12}$ is a cartesian tensor whose elements are

$$(D_{12})_{ij} = -\frac{3x_ix_j - \delta_{ij}r^2}{r^5}\frac{\mu_1\mu_2}{I_1 I_2}. \tag{12}$$

and where I_1 and I_2 are the nuclear spins and μ_1 and μ_2 the corresponding magnetic dipole moments. This hamiltonian can be rewritten in the form of spherical tensors as

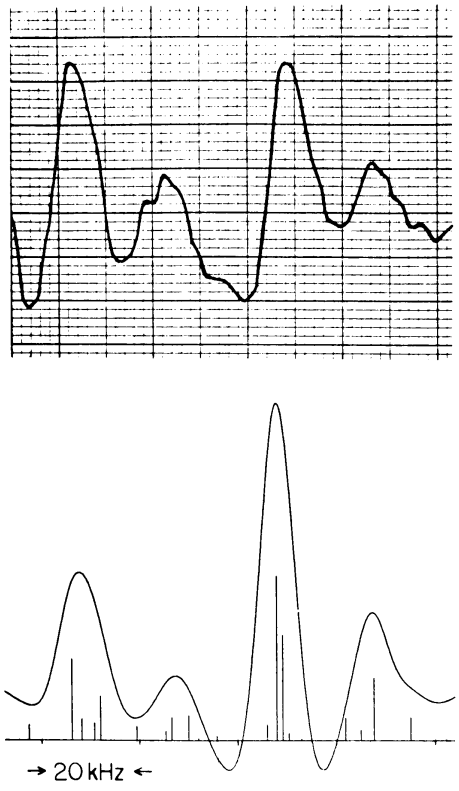

Figure 4. Experimental and theoretical spectrum for the $F_N = 2 \rightarrow 2$ of the $1_{11} \rightarrow 1_{01}$ transition of ND_2H.

$$\mathbf{I}_1 \cdot \mathbf{D}_{12} \cdot \mathbf{I}_2 = -\sqrt{\tfrac{5}{2}} I_1^{(1)} \cdot (D_{12}^{(2)} \times I_2^{(1)})^{(1)}$$
$$= \sqrt{\tfrac{3}{2}} D^{(2)} \cdot (I_1^{(1)} \times I_2^{(1)})^{(2)}, \quad (13)$$

where $D^{(2)}$ is a second-rank spherical tensor with $D_0^{(2)} = D_{zz}$ and $\langle JJ|D_0^{(2)}|JJ\rangle$ is the spin–spin parameter SS. The matrix elements of the hamiltonian written in spherical operator form can be derived by the techniques of reference [12].

The hamiltonian of equation (7) results in a total of 18 hyperfine constants in addition to the unsplit rotational frequency ν_0. The eight spin–spin parameters can be calculated to within experimental uncertainty from the known molecular geometry. In addition, first approximations to the four nitrogen constants and the unsplit centre frequency ν_0 may be obtained from measurements of the absorption spectra in which none of the hydrogen or deuterium hyperfine structure is resolvable. Since F_N is to a high approximation a good quantum number, the $F_N = 0$ levels of both the 1_{11} and 1_{01} states are unsplit by either the hydrogen or deuterium interaction, and the structure of the $F_N = 1 \rightarrow 0$ and $F_N = 0 \rightarrow 1$ multiplets should be particularly simple. Since the $F_N = 1 \rightarrow 0$ shows two well-resolved lines, whose widths are approximately equal to the spectrometer resolution, it may be inferred that the deuterium quadrupole coupling in the 1_{11} state is quite small and that the observed doublet is due to the hydrogen spin–rotation interaction. This immediately yields $(C_{1_{11}})_H \approx -15$ kHz and $|(eq_{1_{11}}Q)_D| \lesssim 5$ kHz. Similar considerations of the $F_N = 0 \rightarrow 1$ transition yield $(eq_{1_{01}}Q)_D \simeq 30$ kHz. Since the g-factor of deuterium is much smaller than that of hydrogen, it is possible to initially assume that $(C_{1_{11}})_D = (C_{1_{01}})_D = 0$.

This approach gives an adequate approximation of the spectrum to assign most of the major features. The final set of spectroscopic constants was calculated by means of a non-linear least squares analysis. Inspection of figures

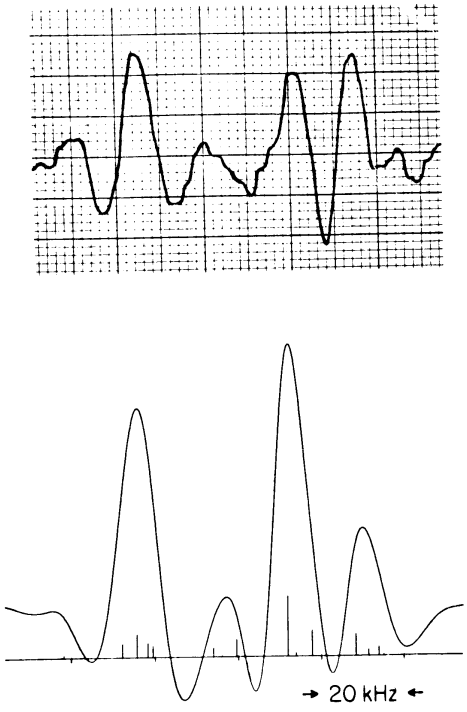

Figure 5. Experimental and theoretical spectrum for the $F_N = 1 \rightarrow 2$ of the $1_{11} \rightarrow 1_{01}$ transition of ND_2H.

1–6 shows that most of the observed lines have contributions from several unresolved transitions. The coefficient matrix of this least squares analysis (i.e. the $\partial \nu_i/\partial C_j$, where the ν_i are the observed frequencies and the C_j are the spectral constants) was calculated by adding ΔC_j to each C_j, computing the shift in the line centre $\Delta \nu_i$ and by setting

$$\Delta \nu_i/\Delta C_j = \frac{\partial \nu_i}{\partial C_j}. \tag{14}$$

These, combined with the calculated differences between the observed and theoretical spectra, formed the basis for the analysis. Constraint equations among the spectral constants could be introduced and the eight spin–spin constants were fixed at their geometric values. The data points were weighted according to estimates both of their experimental uncertainty and of uncertainties produced by unresolved structure, saturation and state selection effects. Since the $\partial \nu_i/\partial C_j$ depend upon the values of the spectral constants, the above procedure was iterated until the values of spectral constants converged.

3.3. *Results*

The beam maser spectrum of ND_2H for $1_{11} \rightarrow 1_{01}$ is shown in figures 1–6. Also shown in figures 1–6 is a theoretical spectrum which was calculated from the hyperfine constants shown in table 1. Agreement between the observed and calculated lines is 1–2 kHz for the splittings which arise from the hydrogen and deuterium interactions and approximately twice that for the splittings which arise from the nitrogen hyperfine interactions. These latter measurements depend

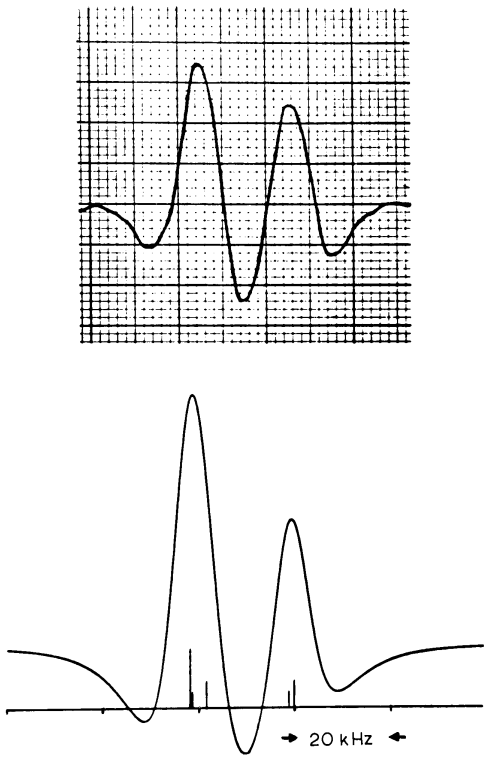

Figure 6. Experimental and theoretical spectrum for the $F_N = 1 \rightarrow 0$ of the $1_{11} \rightarrow 1_{01}$ transition of ND_2H.

	1_{11}	1_{01}
$(eqQ)_N$	$-359{\cdot}4 \pm 0{\cdot}5$ (*d*)	$-408{\cdot}8 \pm 0{\cdot}5$
C_N	$4{\cdot}5 \pm 0{\cdot}5$	$3{\cdot}4 \pm 0{\cdot}5$
$(eqQ)_D$	$-3{\cdot}5 \pm 2{\cdot}0$	$32{\cdot}6 \pm 1{\cdot}0$
C_D (*b*)	$-1{\cdot}5$	$-1{\cdot}9$
C_H	$-16{\cdot}9 \pm 0{\cdot}5$	$-12{\cdot}5 \pm 2{\cdot}0$
SS_{DD} (*c*)	$-0{\cdot}133$	$0{\cdot}267$
SS_{DN} (*c*)	$-0{\cdot}042$	$0{\cdot}246$
SS_{HN} (*c*)	$1{\cdot}879$	$-1{\cdot}695$
SS_{HD} (*c*)	$1{\cdot}008$	$-0{\cdot}217$

Table 1. Hyperfine constants of the 1_{11} and 1_{01} rotational energy levels of ND_2H(kHz) (*a*).

(*a*) Rotational transition frequency is 57 674 491 kHz.
(*b*) Calculated from $(C_H)_{1_{11}}$ and NH_3 results.
(*c*) Calculated from geometry.
(*d*) Quoted errors represent two standard deviations.

upon absolute frequency measurements and the larger deviations may be attributed to cavity pulling effects. Inspection of figures 1–6 shows that most of the lines are made up of a number of unresolved transitions. Several experimental effects may modify the intensities of certain of these transitions, leading to modified line intensities and in some cases shifted line frequencies. Power saturation, a consideration in any beam experiment, may cause shifts in line frequency of several kHz accompanied by similar intensity changes. Figure 7 provides a good demonstration of this effect. The upper tracing was recorded

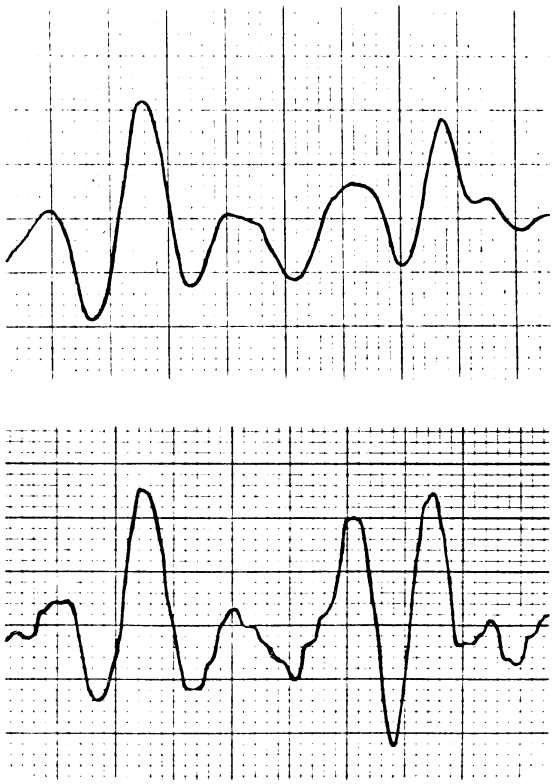

Figure 7. Saturation effects in the spectrum of ND_2H.

at approximately five times the power level of the lower tracing. In this particular case valuable information about two weak lines may be obtained from the high power run, but saturation of the stronger transitions significantly modified much of the rest of the spectrum. Care was taken to record spectral features at a power level consistent with the theoretical model.

The relative intensities of lines measured in a beam maser experiment also depend upon the relative efficiency of state selection. This is of minimal concern for two reasons : the most significant intensity differences occur between widely spaced hyperfine levels (e.g. the nitrogen splitting in ammonia) so that intensity variations which do occur due to state selection efficiencies tend to be between multiplets rather than within multiplets. Furthermore, Majorana transitions [16], which result from the non-adiabatic transition of the molecular beam from the high-field region of the state selector into the zero-field region of the cavity, tend to equalize, within the multiplets, any population differences caused by state selection effects. Although the above effects may cause significant experimental uncertainties, the good agreement between observed and calculated spectra indicates that the problem is not a major one.

4. Hyperfine structure of the inversion spectrum of ND_3

4.1. *Review of previous work*

In a previous paper Hougen [17] has eliminated a number of inconsistencies in previous analyses of $^{14}NH_3$ and $^{15}NH_3$ and a consistent picture of the hyperfine coupling has emerged for these species. Studies of ND_3 should provide valuable information about the deuterium quadrupole coupling which is unobtainable from studies of NH_3 as well as confirm expected isotopic relationships between spectroscopic constants of the two species. Zuev [8] has studied the hyperfine structure of the $J=K=6$ inversion transition at 1656·18 MHz. Considerable theoretical work on this transition has been done by Svidzinskii [11] and a preliminary analysis has been reported. However, it was not possible to achieve a satisfactory agreement between the experimental and theoretical results [7]. As a result, Basov and Bashkin [7] undertook a study of the $J=K=4$ transition. This spectrum is simpler because of fewer allowed spin states. Figure 8 shows a comparison of the experimental and theoretical results of Basov and Bashkin. It can be seen that the discrepancies between the observed and calculated spectrum are large.

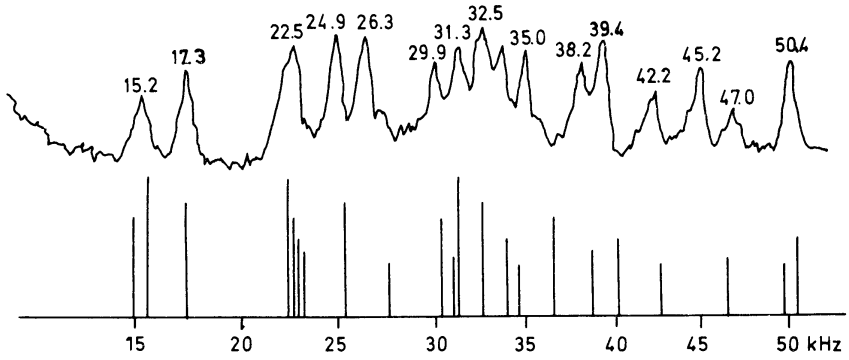

Figure 8. Experimental and theoretical spectrum of the $J=K=4$ inversion transition of ND_3 from reference [7].

4.2. *Theoretical considerations*

In a molecule containing identical atoms in identical sites, the coupling scheme which is most useful is one in which these nuclear spins are first coupled together to form a resultant, which in turn is coupled to the other nuclei in the fashion of reference [12]. In the case of ND_3 the three spin-1 deuterium nuclei form the five distinct coupled spin states of table 2. The overall symmetry type must be A_1 (since the deuterons are bosons), so the E spin states can occur only with the type-E rotational states $|K| = 1, 2 \pmod 3$, and the A_1 and A_2 states with $|K| = 0 \pmod 3$. Since we are only concerned with a first-order treatment of the hyperfine interactions (with respect to the rotation–inversion states), we need only consider matrix elements of these interactions which are diagonal in the spin state symmetry type, but this still allows off-diagonal elements in the resultant spin.

The hyperfine interactions in ND_3 have to be resolved into terms which are classified as products of irreducible tensors of both the symmetry type and the angular momentum according to the techniques of reference [10], and take the following form :

$$\mathscr{H}Q_N = \tfrac{1}{2}V_2^{A_1}(N) : Q_2^{A_1}(N), \tag{15}$$

$$\mathscr{H}SR_N = \mathbf{I}(N) \,.\, \mathbf{C}(N) \,.\, \mathbf{J}$$
$$= \{[C_0^{A_1}(N) \times J_1^{A_1}]_1^{A_1} - (\tfrac{5}{2})^{1/2}[C_2^{A_1}(N) \times J_1^{A_1}]_1^{A_1}\} : I_1^{A_1}(N), \tag{16}$$

$$\mathscr{H}Q_D = \tfrac{1}{2}V_2^{A_1}(D) : Q_2^{A_1}(D) + \tfrac{1}{2}V_2^{E}(D) : Q_2^{E}(D), \tag{17}$$

$$\mathscr{H}SR_D = \sum_i \mathbf{I}(D_i) \,.\, \mathbf{C}(D_i) \,.\, \mathbf{J}$$
$$= \{[C_0^{A_1}(D) \times J_1^{A_1}]_1^{A_1} + [C_1^{A_1}(D) \times J_1^{A_1}]_1^{A_1} - (\tfrac{5}{2})^{1/2}[C_2^{A_1}(D) \times J_1^{A_1}]_1^{A_1}\} : I_1^{A_1}(D) + \{[C_0^{E}(D) \times J_1^{A_1}]_1^{E} + [C_1^{E}(D) \times J_1^{A_1}]_1^{E} - (\tfrac{5}{2})^{1/2}[C_2^{E}(D) \times J_1^{A_1}]_1^{E}\} : I_1^{E}(D), \tag{18}$$

$$\mathscr{H}SS_{ND} = \sum_i \mathbf{I}(N) \,.\, \mathbf{D}(ND_i) \,.\, \mathbf{I}(D_i)$$
$$= \{[D_0^{A_1}(ND) \times I_1^{A_1}(N)]_1^{A_1} - (\tfrac{5}{2})^{1/2}[D_2^{A_1}(ND) \times I_1^{A_1}(N)]_1^{A_1}\} : I_1^{A_1}(D) + \{[D_0^{E}(ND) \times I_1^{A_1}(N)]_1^{E} - (\tfrac{5}{2})^{1/2}[D_2^{E}(ND) \times I_1^{A_1}(N)]_1^{E}\} : I_1^{E}(D), \tag{19}$$

$$\mathscr{H}SS_{DD} = \mathbf{I}(D_2) \,.\, \mathbf{D}(D_2D_3) \,.\, \mathbf{I}(D_3) + \mathbf{I}(D_3) \,.\, \mathbf{D}(D_3D_1) \,.\, \mathbf{I}(D_1) + \mathbf{I}(D_1) \,.\, \mathbf{D}(D_1D_2) \,.\, \mathbf{I}(D_2)$$
$$= D_0^{A_1}(DD) : T_0^{A_1} + D_2^{A_1}(DD) : T_2^{A_1} + D_0^{E}(DD) : T_0^{E} + D_2^{E}(DD) : T_2^{E}. \tag{20}$$

Here the rotation-dependent operators (V, C, and D) of the identical nuclei are given by the forms

$$V^{A_1}(D) = \tfrac{1}{3}\sum_i \mathbf{V}(D_i), \tag{21}$$

$$V^{E+1}(D) = \tfrac{1}{3}[\mathbf{V}(D_1) + \epsilon^2\mathbf{V}(D_2) + \epsilon\mathbf{V}(D_3)], \tag{22}$$

$$D^{E+1}(DD) = \tfrac{1}{3}[\mathbf{D}(D_2D_3) + \epsilon^2\mathbf{D}(D_3D_1) + \epsilon\mathbf{D}(D_1D_2)], \tag{23}$$

etc., where $\epsilon = \exp(i2\pi/3)$, and the spin operators (Q, I, and T) are

$$Q^{A_1}(D) = \sum_i \mathbf{Q}(D_i), \tag{24}$$

$$Q^{E+1}(D) = \mathbf{Q}(D_1) + \epsilon^2 \mathbf{Q}(D_2) + \epsilon \mathbf{Q}(D_3), \tag{25}$$

$$T_{00}{}^{A_1 0} = \mathbf{I}(D_2) \cdot \mathbf{I}(D_3) + \mathbf{I}(D_3) \cdot \mathbf{I}(D_1) + \mathbf{I}(D_1) \cdot \mathbf{I}(D_2), \tag{26}$$

$$T_{00}{}^{E+1} = \mathbf{I}(D_2) \cdot \mathbf{I}(D_3) + \epsilon^2 \mathbf{I}(D_3) \cdot \mathbf{I}(D_1) + \epsilon \mathbf{I}(D_1) \cdot \mathbf{I}(D_2), \tag{27}$$

$$T_{20}{}^{A_1 0} = \tfrac{3}{2}[I_z(D_2)I_z(D_3) + I_z(D_3)I_z(D_1) + I_z(D_1)I_z(D_2)] - \tfrac{1}{2}T_{00}{}^{A_1 0}, \tag{28}$$

$$T_{20}{}^{E+1} = \tfrac{3}{2}[I_z(D_2)I_z(D_3) + \epsilon^2 I_z(D_3)I_z(D_1) + \epsilon I_z(D_1)I_z(D_2)] - \tfrac{1}{2}T_{00}{}^{E+1}, \tag{29}$$

etc. The normalization of the spherical tensor components is such that

$$U_{00} = \tfrac{1}{3}(U_{xx} + U_{yy} + U_{zz}), \tag{30}$$

$$U_{10} = i(2)^{-1/2}(U_{xy} - U_{yx}), \tag{31}$$

$$U_{20} = U_{zz} - U_{00}. \tag{32}$$

The tensor components belonging to the -1 row of the E representation are obtained from the $+1$ components by simple complex conjugation of the coefficients. It should be noted that the rank-one components of the spin–rotation tensor do not contribute to the matrix elements diagonal in $|K|$, but do enter in the asymmetric isotopic forms of the molecule. The direct spin–spin interaction is traceless, so that the scalar components are usually neglected, but must be included if the indirect (electron coupled) contribution is significant.

The terms of the hamiltonian are reduced through the coupling scheme, which in this case involves only

$$\mathbf{J} + \mathbf{I}_N = \mathbf{F}_N, \tag{33 a}$$

$$\mathbf{F}_N + \mathbf{I}_D = \mathbf{F}. \tag{33 b}$$

This gives each of the matrix elements of each of the hyperfine interactions in terms of a product of reduced matrix elements, one of a spin operator and one of an orientation operator. The latter depends on the rotation state, and can be evaluated exactly as in reference [10]. In the present normalization they are

$$\left\langle |K| \begin{matrix}\alpha \\ J\end{matrix} \middle\| U_0{}^{A_1} \middle\| |K| \begin{matrix}\alpha \\ J\end{matrix} \right\rangle = [\alpha]^{1/2}(2J+1)^{1/2} U_{00}(D_1), \tag{34}$$

$$\left\langle |K| \begin{matrix}\alpha \\ J\end{matrix} \middle\| U_2{}^{A_1} \middle\| |K| \begin{matrix}\alpha \\ J\end{matrix} \right\rangle = [\alpha]^{1/2} \left[\frac{3K^2}{J(J+1)} - 1\right] \left[\frac{2J(2J+1)(2J+2)}{(2J-1)(2J+3)}\right]^{1/2} \times \frac{U_{zz}(D_1) - U_{00}(D_1)}{2}, \tag{35}$$

$$\left\langle |K| \begin{matrix}\alpha \\ J\end{matrix} \middle\| U_l{}^{E} \middle\| |K| \begin{matrix}\alpha \\ J\end{matrix} \right\rangle = [\alpha]^{1/2}(-)^{J+v} \left[\frac{2J(2J+1)(2J+2)}{(2J-1)(2J+3)}\right]^{1/2} \times \frac{U_{xx}(D_1) - U_{yy}(D_1)}{4} \delta_{\alpha E} \delta_{l2} \delta_{|K|1}, \tag{36}$$

where the z axis is the molecular symmetry axis and atom D_1 is in the xz plane. For the $\mathscr{H}SS_{DD}$ term $D(D_2D_3)$ would replace $U(D_1)$. The symbol $[\alpha]$ denotes the order of the α irreducible representation of the point group, and is equal to 1 for A_1 and A_2 states and 2 for E states.

The spin-dependent reduced matrix elements have to be evaluated by using the explicit expressions for each of the states in table 2, either in terms of the separate m_I states as in reference [10] or by use of an intermediate coupling angular momentum quantum number as in reference [11]. The required matrix elements are given in table 3.

As an example of the reduction process, consider the matrix elements of the deuterium quadrupole interaction as needed for the $J=|K|=4$ inversion transition :

$$\begin{aligned}
&\left\langle \begin{matrix} E & E & (E) & A_1 \\ J & F_N' & (I_D') & F \end{matrix} \middle\| V_2^{A_1} \cdot Q_2^{A_1} \middle\| \begin{matrix} E & E & (E) & A_1 \\ J & F_N & (I_D) & F \end{matrix} \right\rangle \\
&\quad = (-1)^{I_D+F_N'+F} \begin{Bmatrix} E & E & A_1 \\ E & E & A_1 \end{Bmatrix} \begin{Bmatrix} F_N' & F_N & 2 \\ I_D & I_D' & F \end{Bmatrix} \left\langle \begin{matrix} E \\ I_D' \end{matrix} \middle\| Q_2^{A_1} \middle\| \begin{matrix} E \\ I_D \end{matrix} \right\rangle \\
&\qquad \times (-1)^{J+I_N+F_N+2} 2[(2F_N'+1)(2F_N+1)]^{1/2} \begin{Bmatrix} E & E & A_1 \\ E & E & A_1 \end{Bmatrix} \begin{Bmatrix} J & F_N' & I_N \\ F_N & J & 2 \end{Bmatrix} \\
&\qquad \times \left\langle \begin{matrix} |K| & E \\ J & \end{matrix} \middle\| V_2^{A_1} \middle\| \begin{matrix} |K| & E \\ J & \end{matrix} \right\rangle \\
&\quad = (-1)^{J+I_N+F_N+F_N'+I_D+F} [(2F_N'+1)(2F_N+1)]^{1/2} \begin{Bmatrix} F_N' & F_N & 2 \\ I_D & I_D' & F \end{Bmatrix} \\
&\qquad \times \begin{Bmatrix} J & F_N' & I_N \\ F_N & J & 2 \end{Bmatrix} \tfrac{1}{2} \left\langle \begin{matrix} E \\ I_D' \end{matrix} \middle\| Q_2^{A_1} \middle\| \begin{matrix} E \\ I_D \end{matrix} \right\rangle \left\langle \begin{matrix} |K| & E \\ J & \end{matrix} \middle\| V_2^{A_1} \middle\| \begin{matrix} |K| & E \\ J & \end{matrix} \right\rangle . \qquad (37)
\end{aligned}$$

The factor of $\frac{1}{2}$ in the last line above comes from collecting all the contributions from the point-group reduction formula, and is listed in table 3 with the name ' point-group coupling factor '.

4.3. *Analysis and results*

Inspection of figures 9 and 10 shows that the hyperfine structure of ND_3 is complex. Although the number of spectral constants which characterize its spectra is small compared to the number necessary for ND_2H, it is important to be able to estimate initially as many of these parameters as possible. Studies of NH_3 have shown that the electron-coupled spin–spin interaction is small in ammonia and that spin–spin constants calculated from geometry are accurate. The spin–rotation constant C_D for ND_3 can be calculated from the NH_3 value via equations (4) and (6). This leaves only the deuterium quadrupole constant $(eqQ)_D$ as an adjustable parameter. A value of $(eqQ)_D$ which makes possible the assignment of most of the lines is readily found by straightforward adjustment of this parameter.

This initial assignment makes possible an iterative, non-linear least squares fit (§ 3.2) with $(eqQ)_D$, C_D, SS_{ND} and SS_{DD} as variables. The coefficients of these parameters $\partial\nu_i/\partial C_j$, where the ν_i are the line frequencies and the C_j the spectral constants, were obtained by applying the eigenvector matrices which

$$\left|\begin{matrix} A_1 & 0 \\ 3 & 3 \end{matrix}\right\rangle = |1, 1, 1\rangle$$

$$\left|\begin{matrix} E & +1 \\ 2 & 2 \end{matrix}\right\rangle = (3)^{-1/2}[|0, 1, 1\rangle + \epsilon^2|1, 0, 1\rangle + \epsilon|1, 1, 0\rangle]$$

$$\left|\begin{matrix} A_1 & 0 \\ 1 & 1 \end{matrix}\right\rangle = (15)^{-1/2}\{2[|-1, 1, 1\rangle + |1, -1, 1\rangle + |1, 1, -1\rangle] - [|1, 0, 0\rangle + |0, 1, 0\rangle + |0, 0, 1\rangle]\}$$

$$\left|\begin{matrix} E & +1 \\ 1 & 1 \end{matrix}\right\rangle = (6)^{-1/2}[|-1, 1, 1\rangle + \epsilon^2|1, -1, 1\rangle + \epsilon|1, 1, -1\rangle + |1, 0, 0\rangle + \epsilon^2|0, 1, 0\rangle + \epsilon|0, 0, 1\rangle]$$

$$\left|\begin{matrix} A_2 & 0 \\ 0 & 0 \end{matrix}\right\rangle = (6)^{-1/2}[|1, 0, -1\rangle + |-1, 1, 0\rangle + |0, -1, 1\rangle - |1, -1, 0\rangle - |0, 1, -1\rangle - |-1, 0, 1\rangle]$$

The remaining m_I values are obtained by use of the ladder operators, and the states belonging to the -1 row of the E representation are obtained by complex conjugation of the coefficients in those for the $+1$ row. The symbol ϵ stands for the complex number $\exp(i2\pi/3)$.

Table 2. Deuterium spin states of ND_3 : $\left|\begin{matrix} \alpha & \mu \\ I_D & m_I \end{matrix}\right\rangle$.

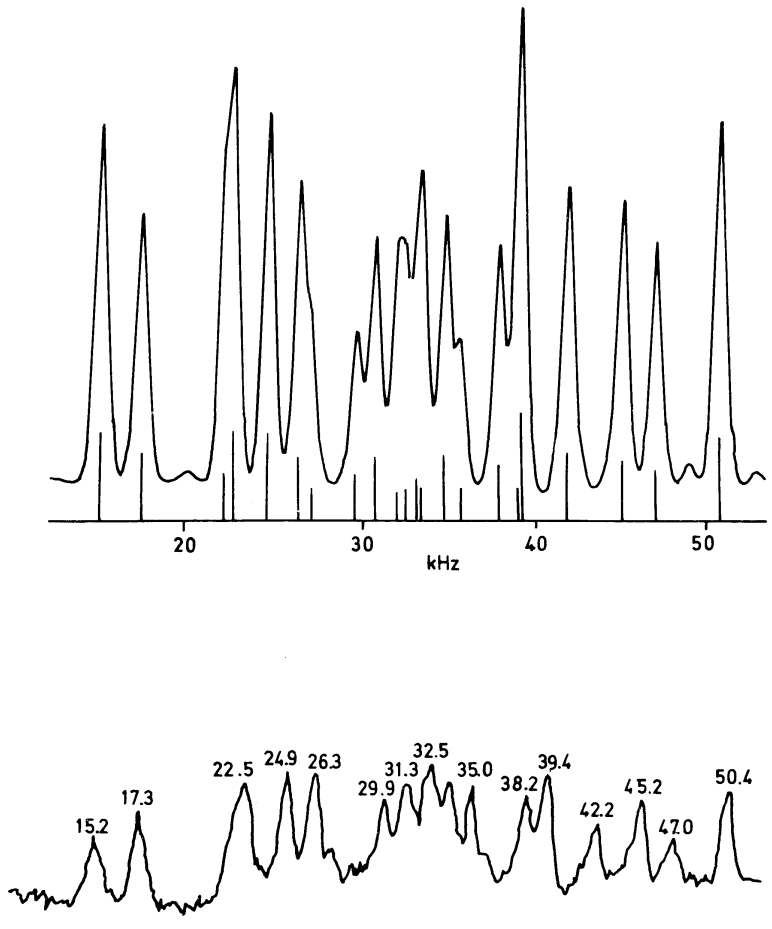

Figure 9. Comparison of the experimental spectrum of the $J=K=4$ inversion transition of ND_3 from reference [7] and the theoretical results of this work.

Nitrogen spin operators

$$\left\langle \begin{matrix} A_1 \\ I_N \end{matrix} \middle\| \; I_1{}^{A_1}(\mathrm{N}) \; \middle\| \begin{matrix} A_1 \\ I_N \end{matrix} \right\rangle = \tfrac{1}{2}[2I_N(2I_N+1)(2I_N+2)]^{1/2}$$

$$\left\langle \begin{matrix} A_1 \\ I_N \end{matrix} \middle\| \; Q_2{}^{A_1}(\mathrm{N}) \; \middle\| \begin{matrix} A_1 \\ I_N \end{matrix} \right\rangle = \frac{eQ_N}{2} \left\{ \frac{(2I_N+1)(2I_N+2)(2I_N+3)}{2I_N(2I_N-1)} \right\}^{1/2}$$

Deuterium spin operators

λ	α	I_D'	I_D	$\left\langle \begin{matrix} \alpha \\ I_D' \end{matrix} \middle\| I_1{}^{\lambda}(D) \middle\| \begin{matrix} \alpha \\ I_D \end{matrix} \right\rangle$	$\left\langle \begin{matrix} \alpha \\ I_D' \end{matrix} \middle\| Q_2{}^{\lambda}(D) \middle\| \begin{matrix} \alpha \\ I_D \end{matrix} \right\rangle$	$\left\langle \begin{matrix} \alpha \\ I_D' \end{matrix} \middle\| T_2{}^{\lambda} \middle\| \begin{matrix} \alpha \\ I_D \end{matrix} \right\rangle$
A_1	A_1	3	3	$(84)^{1/2}$	$eQ_D(189/5)^{1/2}$	$(756/5)^{1/2}$
		3	1	0	$eQ_D(126/5)^{1/2}$	$-(63/10)^{1/2}$
		1	3	0	$eQ_D(126/5)^{1/2}$	$-(63/10)^{1/2}$
		1	1	$(6)^{1/2}$	$eQ_D(243/10)^{1/2}$	$-(6/5)^{1/2}$
A_1	E	2	2	$(60)^{1/2}$	0	$(315/4)^{1/2}$
		2	1	0	$eQ_D(45)^{1/2}$	$-(45/4)^{1/2}$
		1	2	0	$-eQ_D(45)^{1/2}$	$(45/4)^{1/2}$
		1	1	$(12)^{1/2}$	0	$(15/4)^{1/2}$
A_1	A_2	0	0	0	0	0
E	E	2	2	$-(15)^{1/2}$	$-eQ_D(315/4)^{1/2}$	0
		2	1	$-(45)^{1/2}$	$-eQ_D(45/4)^{1/2}$	$(45)^{1/2}$
		1	2	$(45)^{1/2}$	$eQ_D(45/4)^{1/2}$	$-(45)^{1/2}$
		1	1	$-(3)^{1/2}$	$eQ_D(135/4)^{1/2}$	$(60)^{1/2}$

Rotation dependent operators

$$\left\langle |K| \begin{matrix} \alpha \\ J \end{matrix} \middle\| \; J_1{}^{A_1} \; \middle\| |K| \begin{matrix} \alpha \\ J \end{matrix} \right\rangle = [\alpha]^{1/2}\tfrac{1}{2}[2J(2J+1)(2J+2)]^{1/2}$$

$$\left\langle |K| \begin{matrix} \alpha \\ J \end{matrix} \middle\| \; (C_0{}^{A_1} \times J_1{}^{A_1})_1{}^{A_1} - (\tfrac{5}{2})^{1/2}(C_2{}^{A_1} \times J_1{}^{A_1})_1{}^{A_1} \; \middle\| |K| \begin{matrix} \alpha \\ J \end{matrix} \right\rangle$$

$$= \tfrac{1}{2}C_J[\alpha]^{1/2}[2J(2J+1)(2J+2)]^{1/2}$$

$$\left\langle |K| \begin{matrix} \alpha \\ J \end{matrix} \middle\| \; -(\tfrac{5}{2})^{1/2}(C_2{}^{E} \times J_1{}^{A1})_1{}^{E} \; \middle\| |K| \begin{matrix} \alpha \\ J \end{matrix} \right\rangle$$

$$= \delta_{|K|1}\delta_{E\alpha}(-)^{J+v}\tfrac{1}{8}(C_{xx}-C_{yy})[\alpha]^{1/2}[2J(2J+1)(2J+2)]^{1/2}$$

Point-group coupling factors

$\mathrm{HQ_N}$ and $\mathrm{HSR_N}$: $[\alpha]^{-1/2}$

$\mathrm{HQ_D}$, $\mathrm{HSR_D}$, $\mathrm{HSS_{ND}}$, $\mathrm{HSS_{DD}}$, A_1 operator terms : $[\alpha]^{-1}$

E operator terms : $(-)^{2I}[\alpha]^{-1}$

(I is the spin of each deuterium nucleus)

Table 3. Reduced matrix elements for ND_3.

diagonalize the hamiltonian to each term of the hamiltonian. Since, in general, the $\partial v_i/\partial C_j$ depend upon the values of the C_j, iteration is required. However, since the nitrogen interaction is significantly larger than the deuterium interaction, the iterated result differs little from the first-order results and the solution converges rapidly.

The hyperfine constants which result from this analysis of the $J=|K|=4$ spectrum are shown in table 4. These constants when combined with intensity calculations, can be used to calculate and plot a theoretical spectrum which can be compared with the experimental data. Inspection of the experimental data reveals that the lineshapes are more triangular than gaussian or lorentzian. It was found that a mixture of one part lorentizan and 0·4 parts second derivative

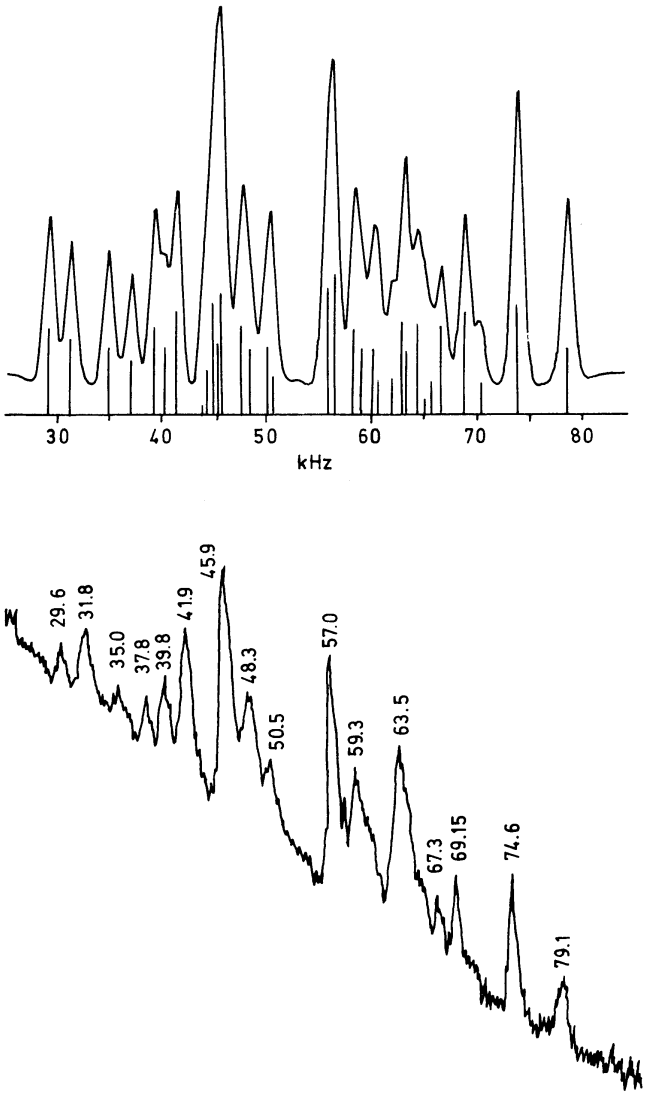

Figure 10. Comparison of the experimental spectrum of the $J=K=6$ inversion transition of ND_3 from reference [8] and the theoretical results of this work.

	$J=\|K\|=4$	$J=\|K\|=6$
$(eqQ)_D$	$-69{\cdot}19\pm0{\cdot}44$ (*a*)	$-95{\cdot}55\pm0{\cdot}67$
C_D	$-1{\cdot}056\pm0{\cdot}04$	$-1{\cdot}437\pm0{\cdot}001$
SS_{DD}	$0{\cdot}40\pm0{\cdot}25$	$0{\cdot}72\pm0{\cdot}08$
SS_{ND}	$0{\cdot}54\pm0{\cdot}29$	$0{\cdot}79\pm0{\cdot}15$

(*a*) Quoted errors represent two standard deviations

Table 4. Hyperfine constants of the inversion spectrum of ND_3 (kHz).

lorentzian gives a good approximation to the observed lineshapes. Figure 9 shows a comparison between the experimental spectrum and our calculated spectrum. It can be seen that the agreement is on the order of the expected experimental error.

A similar procedure was used for the analysis of the hyperfine spectrum of the $J=|K|=6$ transition and the hyperfine constants which result are shown in table 4. The theoretical spectrum is plotted and compared with the experimental spectrum in figure 10. Again the agreement between the experimental and calculated spectra is excellent.

Comparison of the values of $(eqQ)_D$ and C_D for the $J=|K|=4$ and $J=|K|=6$ spectra reveals that they differ significantly. Inspection of figures 9 and 10 shows, however, that the fits of both of these spectra are very good and that an explanation of the difference is unlikely to lie in an alternate assignment of one or both of the spectra. The deuterium quadrupole coupling constant of the $J=|K|=6$ spectrum agrees to approximately 4 per cent with the value calculated by Garvey and De Lucia from the $K=0$, $J=1\rightarrow 0$ beam maser spectrum of ND_3 at 309 GHz [9]. In addition, the value of C_D for $J=|K|=6$ can be calculated from a knowledge of the diagonal terms of the hydrogen tensor. This has been done using the results of Hougen's re-analysis of Kukolich's NH_3 data. The results of this analysis are shown in table 5 and yield, via equation (6), $C_D=$ $=1{\cdot}458$ kHz for the $J=|K|=6$ inversion transitions and $-1{\cdot}455$ kHz for the $J=|K|=4$ inversion transition of ND_3. This value is also in excellent agreement with the results of the $J=|K|=6$ analysis.

$\Lambda_{11}=(-19{\cdot}84\pm 0{\cdot}35)\times 10^{-10}$ (*a*)
$\Lambda_{22}=(-193{\cdot}93\pm 0{\cdot}35)\times 10^{-10}$
$\Lambda_{33}=(-181{\cdot}36\pm 0{\cdot}29)\times 10^{-10}$

(*a*) The $\bar{\Lambda}$ tensor is dimensionless. Errors quoted are two standard deviations.

Table 5. Diagonal elements of the $\bar{\Lambda}_H$ tensor as derived from the hydrogen spin–rotation constants of $^{14}NH_3$ and $^{15}NH_3$.

It is interesting to note that the values predicted for both $(eqQ)_D(J=|K|=4)$ and $C_D(J=|K|=4)$ are within 1 per cent of 1·38 times larger than those calculated from the experimental data. The ratios of the calculated and observed spin–spin constants are also consistent with this ratio although their uncertainties are significantly larger. We would suggest that one possible explanation for the inconsistency between the $J=|K|=6$, the $J=1\rightarrow 0$, $K=0$, and NH_3 data on one hand and the $J=|K|=4$ data on the other could be an error in the dispersion calculation of 1·38 in the $J=|K|=4$ experimental data.

5. Discussion

Although a large number of measurements of the hyperfine structure of the various isotopic species of ammonia have been made, very little work has been reported which investigates the relationships which exist among the spectral constants which have been calculated from these observations. These relations

are useful not only for the calculation of molecular properties of ammonia, but also as a check of the experimental results. A convenient coordinate system for these comparisons is defined in figure 11.

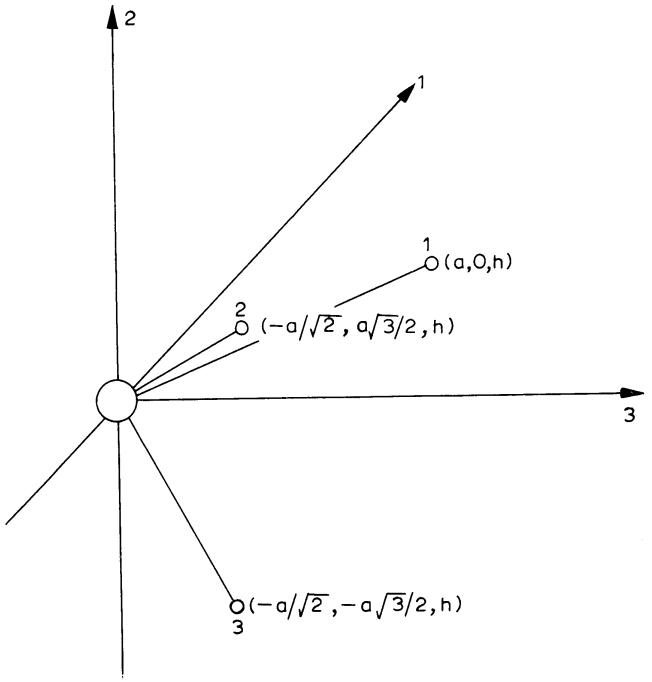

Figure 11. Ammonia geometry in the 1, 2, 3 symmetry system.

5.1. *Nitrogen quadrupole*

The re-interpretation of Kukolich's [2–4] data by Hougen [17] leads to a consistent picture of the role of the nitrogen quadrupole coupling in $^{14}NH_3$ and $^{15}NH_3$. Since the nitrogen nucleus lies on the axis of symmetry, the form of its quadrupole coupling tensor is†

$$\begin{pmatrix} V_{11} & 0 & 0 \\ 0 & V_{22} & 0 \\ 0 & 0 & V_{33} \end{pmatrix}$$

with $V_{11} = V_{22} = -\frac{1}{2}V_{33}$. Consequently, one number defines the quadrupole coupling and, under the assumption of constant electronic structures, its value is unchanged by isotopic substitution of the hydrogen atoms.

Table 6 shows a comparison between the observed spectral constants of the several experiments and the value of these constants calculated by the techniques of § 2 from $(eqQ)_N = -4090$ kHz. This table shows that the results of the absorption studies of the inversion spectrum of ND_3 by Hermann [20], the submillimetre beam maser measurements of ND_3 by Garvey and De Lucia [9], the NH_2D work of Kukolich [6], and the ND_2H work reported in this paper

† Certain higher order effects discussed by Hougen have little or no observable effects in the spectra discussed here (except for NH_3) and are therefore not considered.

agree to about 0·2 per cent with the results calculated from the NH_3 value. The slight trend toward smaller coupling constants with increased reduced mass is probably real and is similar to the decrease found for the nitrogen quadrupole coupling in HCN [18]. A rather large disagreement exists between the value calculated directly from the 3_{13}–3_{03} spectrum of NH_2D and the value calculated from the molecular tensor.

	Observed	Calculated from NH_3	Reference
ND_3			
(eQq) (a)	-4080 ± 3	-4090	[20]
$(eQq)_{J=5,\ \lvert K\rvert=3}$	-4023 ± 22	-4090	[7]
$(C_J)_{J=5,\ \lvert K\rvert=3}$	$3{\cdot}5 \pm 0{\cdot}3$	3·47	[7]
ND_2H			
$(eQq_J)_{1_{11}}$	$-359{\cdot}4 \pm 0{\cdot}5$	$-360{\cdot}40$	(*b*)
$(eQq_J)_{1_{01}}$	$-408{\cdot}8 \pm 0{\cdot}5$	$-409{\cdot}00$	(*b*)
$C(1_{11})$	$4{\cdot}5 \pm 0{\cdot}5$	4·51	(*b*)
$C(1_{01})$	$3{\cdot}4 \pm 0{\cdot}5$	3·84	(*b*)
NH_2D			
$(eQq_J)_{4_{14}}$	$-1895{\cdot}65 \pm 0{\cdot}7$	$-1901{\cdot}49$	[6]
$(eQq_J)_{4_{04}}$	$-1811{\cdot}55 \pm 0{\cdot}7$	$-1816{\cdot}74$	[6]
$\frac{C(4_{14})+C(4_{04})}{2}$	$5{\cdot}027 \pm 0{\cdot}18$	4·969	[6]
$C(4_{14})-C(4_{04})$	$0{\cdot}062 \pm 0{\cdot}018$	0·051	[6]
$(eQq_J)_{3_{13}}-(eQq_J)_{3_{03}}$	$-197{\cdot}3 \pm 0{\cdot}6$	$-191{\cdot}92$	[5]
$C(3_{13})-C(3_{03})$	$0{\cdot}3 \pm 0{\cdot}2$	0·15	[5]

(*a*) The observed value was calculated from an analysis of several J, K states.
(*b*) This work.

Table 6. A comparison of the observed nitrogen hyperfine coupling constants.

Bashkin [19] has attempted to study the effects of deuterium substitution on the nitrogen quadrupole coupling constant by examination of the $J=5$, $|K|=3$ state of the ND_3 inversion spectrum at 1509 MHz. This state was chosen because the factor $3K^2/J(J+1)-1$ which enters into the deuterium quadrupole energy expression is only 0·1 for this state. As a result, the deuterium hyperfine structure was not resolvable, thus avoiding the complexities associated with an analysis of the hyperfine structure of three identical deuterium nuclei. Unfortunately, the nitrogen quadrupole coupling is reduced by a like amount and it is not possible to calculate the value of $(eq_JQ)_N$ to a high accuracy from this spectrum. Consequently, it would seem reasonable to attribute this discrepancy to experimental uncertainty rather than to an isotope effect.

5.2. *Nitrogen spin–rotation*

The nitrogen spin–rotation interaction is significantly smaller than the nitrogen quadrupole interaction. The form of its coupling tensor is

$$\begin{pmatrix} C_{11} & 0 & 0 \\ 0 & C_{22} & 0 \\ 0 & 0 & C_{33} \end{pmatrix}$$

with $C_{11} = C_{22}$. This tensor is not invariant under isotopic substitution, but the $\mathbf{\Lambda}$ tensor, whose elements are given by $\Lambda_{gg} = C_{gg}/B_g g_I$, is invariant.

Table 6 shows a comparison between the coupling constants obtained directly from the experimental data and those calculated from the $^{14}NH_3$ and $^{15}NH_3$ data via equations (4) and (6).

Inspection of this table shows that all of the spectroscopic constants obtained from the various isotopic species agree with these calculated values to within quoted experimental uncertainty.

5.3. *Hydrogen spin–rotation*

The diagonal elements of the $\mathbf{\Lambda}$ tensor for ammonia can be calculated from the spectroscopic constants of $^{14}NH_3$, $^{15}NH_3$, and $^{14}ND_3$. The results of such an analysis are shown in Table V. Although this analysis results in accurate values of the Λ_{ii}, it is not possible to reproduce the observed spectra to within expected experimental uncertainty. This is not unexpected because of the high accuracy of the experimental data and the wide range of states involved. It is not unreasonable to attribute these small differences to isotope effects and centrifugal distortion.

For nucleus #1 of figure 11, the form of the $\mathbf{\Lambda}$ tensor is

$$\begin{pmatrix} \Lambda_{11} & 0 & \Lambda_{13} \\ 0 & \Lambda_{22} & 0 \\ \Lambda_{13} & 0 & \Lambda_{33} \end{pmatrix}$$

The value of Λ_{13} can only be calculated from the spectroscopic constants of NH_2D and ND_2H. Calculations based on the spectroscopic constants of the four states of NH_2D that have been studied, do not result in consistent values of Λ_{13} nor do the constants of ND_2H reported in this work. As a result, it would appear that it is not possible to define a $\mathbf{\Lambda}$ tensor for ammonia which does not include effects due to isotopic substitution, centrifugal distortion, and molecular inversion. It has been demonstrated previously that similar, but smaller, effects result from centrifugal distortion in the water molecule [15].

5.4. *Deuterium quadrupole*

Significantly less data exist for this interaction than for any of the others, because the vast majority of beam maser work has been done on the $^{14}NH_3$ and $^{15}NH_3$ isotopic forms. The value of V_{33} can be derived directly from either the

$J=|K|=6$ results obtained in an earlier section or from the results on the $J=1\rightarrow 0$ spectra of Garvey and De Lucia. The excellent agreement of these rather dissimilar experiments would indicate that the value of V_{33} is accurately known. The value of $V_{22}-V_{11}$ can be obtained from Herrman's [20] absorption studies of the $J=1$, $|K|=1$; $J=2$, $|K|=1$; and $J=3$, $|K|=1$ inversion. This coupled with the relation $V_{11}+V_{22}+V_{33}=0$ yields

$$eQV_{11}=\ 178\ \text{kHz},$$

$$eQV_{22}=-82\ \text{kHz},$$

$$eQV_{33}=-96\ \text{kHz}.$$

It would be interesting to study one or more of these transitions by beam maser techniques both to improve the accuracy of these values and to provide some experimental redundancy in the calculation.

As for the hydrogen spin–rotation constant, the deuterium quadrupole coupling tensor has the form

$$\begin{pmatrix} V_{11} & 0 & V_{13} \\ 0 & V_{22} & 0 \\ V_{13} & 0 & V_{33} \end{pmatrix}$$

In principle the value of V_{13} can be calculated from a knowledge of the deuterium quadrupole coupling constant in any state for either NH_2D and ND_2H. However, as in the case of the spin–rotation constant, the values obtained from the various states are not self-consistent.

5.5. *Spin–spin constants*

Because the nuclear g-factor of hydrogen is significantly larger than for deuterium, $^{14}NH_3$ and $^{15}NH_3$ are the most accurate tests of the spin–spin interaction. The recent analysis by Hougen indicates that the effects of the electron-coupled spin–spin interaction are small and that calculations which neglect this effect and which are based entirely on the molecular geometry are accurate. The results from all other isotopic species are consistent with this conclusion.

The authors would like to thank Professor Walter Gordy for his support and encouragement during this project.

References

[1] Gordon, J. P., 1955, *Phys. Rev.*, **99,** 1253.
[2] Kukolich, S. G., 1967, *Phys. Rev.*, **156,** 83.
[3] Kukolich, S. G., 1968, *Phys. Rev.*, **172,** 59.
[4] Kukolich, S. G., and Wofsy, S. C., 1970, *J. chem. Phys.*, **52,** 5477.
[5] Thaddeus, P., Krisher, L. C., and Cahill, P., 1964, *J. chem. Phys.*, **41,** 1542.
[6] Kukolich, S. G., 1968, *J. chem. Phys.*, **49,** 5523.
[7] Basov, N. G., and Bashkin, A. S., 1968, *JETP Lett.*, **8,** 188.
[8] Zuev, V. S., 1962, *Opt. Spektrosk.*, **12,** 641. (1962, *Opt. Spectrosc.*, **12,** 358).
[9] Garvey, R. M., and De Lucia, F. C., (to be published).

[10] CEDERBERG, J. W. 1972, *Am. J. Phys.*, **40,** 159.
[11] SVIDZINSKII, K. K., 1963, *Trudy, fiz. Inst. Akad. Sci.*, **21,** 107.
[12] COOK, R. L., and DE LUCIA, F. C., 1971, *Am. J. Phys.*, **39,** 1433.
[13] THADDEUS, P., KRISHER, L. C., and LOUBSER, J. H. N., 1964, *J. chem. Phys.*, **40,** 169.
[14] THADDEUS, P., and KRISHER, L. C., 1961, *Rev. scient. Instrum.*, **32,** 1083.
[15] DYMANUS, A., 1968, *Physics Lett.*, **26,** A, 424.
[16] MAJORANA, E., 1932, *Nuovo Cim.*, **9,** 43.
[17] HOUGEN, J. T., 1972, *J. chem. Phys.*, **57,** 4207.
[18] DE LUCIA, F. C., and GORDY, W., 1969, *Phys. Rev.*, **187,** 58.
[19] BASHKIN, A. S., 1969, *Opt. Spektrosk.*, **27,** 360. (1969, *Opt. Spectrosc.*, **27,** 190.)
[20] HERRMAN, G. R., 1958, *J. chem. Phys.*, **29,** 875.